12th International Symposium on Turbulence and Shear Flow Phenomena (TSFP12)
Osaka, Japan (Online), July 19-22, 2022

YAWED AHMED BODY: IMPACT OF VERTICAL FLAPS ON FLOW STRUCTURES

Sukruth Satheesh
sukruth.satheesh@univ-poitiers.fr

Laurent Cordier
laurent.cordier@univ-poitiers.fr

Franck Kerhervé
franck.kerherve@univ-poitiers.fr

Andreas Spohn
andreas.spohn@ensma.fr

Département Fluides, Thermique et Combustion, Institut Pprime, UPR 3346 CNRS,
ENSMA, Université de Poitiers, 86360 Futuroscope-Chasseneuil, France

ABSTRACT

The vortical structures and aerodynamic drag generated by an Ahmed body with square back are studied for various yaw angles. To reduce the impact of yaw and drag the rear-end is equipped with two trailing edge flaps along the lateral sides. The experiments combine force measurements and flow visualizations inside a low-speed water tunnel at Reynolds numbers of $\mathcal{O}[10^4]$. Under yaw conditions strong vortical structures form on the rounded front part, while drag increases. Inclining the flaps inwards towards the middle plane of the model leads to a drag reduction of about 2.5%. The results from flow visualization also highlight the yaw dependency of conical vortices existing on the model roof.

INTRODUCTION

Reducing drag and lift of ground vehicles remains a major challenge to improve energy efficiency and thus pollution. The so-called Ahmed body (Ahmed *et al.* (1984)) has become a standard configuration to experiment new techniques in view of aerodynamic improvement. The sharp corners at the rear-end of the Ahmed body with square back lead to massively separated flow and high pressure drag. Therefore, most attempts are directed to increase base pressure along the rear panel. To achieve this goal many recent studies used injection of momentum to do virtual form shaping by acting on the mixing process shortly upstream and downstream of flow separation. Another well-known technique is to change the shape of the rear-end by adding flaps. Flaps allow to increase pressure before flow separation and thus increasing the base pressure. All these techniques must be optimized to get the best compromise between energy expended and/or detrimental geometric deformation of the base configuration. When transposing results from all these studies under controlled flow conditions without yaw to more realistic road conditions, with fluctuating side-wind, the obtained results are often too optimistic. The aim of the present study is to investigate the impact of yaw on the vortical flow structure and drag forces of Ahmed body. In order to minimize the aerodynamic drag under yaw the rear end is equipped with trailing edge flaps along each lateral side. These flaps can be inclined at various angles inward or outward of the middle plane.

Flaps in various configurations and control mechanisms have been studied for drag reduction. However, there are very limited studies that correlate forces to the physics of flow separation, both on the leading and trailing parts of Ahmed-body. This phenomenon is of greater relevance when the body is at an angle with respect to the flow direction (i.e. yaw). The present work therefore focuses on identifying the variation of flow separation regions and their effect on horizontal forces using visualization techniques, on Ahmed body models with square-back configuration and with vertical flaps mounted on lateral edges at a fixed deflection angle.

A significant amount of literature on flaps of various sizes and different configurations, and their effect on generated forces exists. The work by Fourrié *et al.* (2011) presents a detailed explanation regarding the effect of a single horizontal deflector on Ahmed body with a fixed, slanted rear window on lift and drag forces. It indicated existence of an optimum deflector angle at which drag is minimized due to the disruption of counter-rotating vortices generated by the lateral edges. Littlewood & Passmore (2010) studied the effect of chamfering implemented only on a small part of the upper trailing-edge of a bluff body and reported significant drag reduction due to change in flow orientation resulting in higher base pressures. de la Cruz *et al.* (2017) conducted a series of wind tunnel tests on Ahmed body with vertical flaps mounted on the lateral edges over a range of flap angles, with both flaps moving in a symmetric or even an asymmetric manner, and body yaw angles. They found that minimum drag is achieved when the flaps are deflected asymmetrically in cases involving model yaw due to a smoother taper (boat-tailing), resulting in wake size reduction. Grandemange *et al.* (2015) have conducted wind tunnel experiments to look at the effect of chamfering the top and bottom sections of the base region of a square-back Ahmed body over different yaw angles, and found that chamfering contributes significantly to drag reduction. Beaudoin & Aider (2008) have studied a range of deflectors operating in various combinations, and their effect on lift and drag on a Ahmed body with a slant-back. They found that vertical deflectors mounted about the slant surface have greatest effect in reducing drag and lift due to recirculation area enlargement.

They also report that vertical flaps operating in tandem with other specific flaps offer greater force reduction when compared only to vertical ones. In a recently published study, Tran *et al.* (2022) have performed force and skin-friction measurements on a slant-back Ahmed body in yaw. Their drag and lift measurements presents certain distinct characteristics. The plots present minimal changes in drag and lift magnitudes over a small range of angles ($\beta = 0^\circ - \pm 3^\circ$), post which the trends are linear. This hints at yaw insensitivity of forces over a small range of angles. However, no further analyses has been presented to elucidate this aspect.

In all, this indicates that a gap in understanding with regards to the flow topology in a yawed Ahmed body. The focus of this work involving Ahmed body is to identify the effect of vertical flaps on the observed flow structures quantitatively and qualitatively, and comparing it against that presented by a configuration without flaps.

EXPERIMENTAL SETUP

The paper is organized as follows. First, the experimental setup is explained followed with a description and discussion of the drag forces and the flow structures obtained through visualization, for the different Ahmed body configurations tested here. Experiments are conducted in the free-surface water channel Hydra III at Institut Pprime (Poitiers, France). The overall test section- 2.1 m long and 0.51$\times$ 0.33 m^2 in cross-section is made of glass windows to allow optical access, with the freestream velocity ranging from 0.05 to 0.45 ms^{-1}. A square-back Ahmed body model (0.292 (l)$\times$ 0.109 (w)$\times$ 0.0806 (h) m) is installed in the front portion of the test section. The model is mounted on a plate to replicate the effect of ground, with the leading edge of the plate located $\sim 0.65h$ ahead of the model. The leading edge of the plate is chamfered to fix and stabilize the front stagnation point, and the height of model legs being $\sim 0.18h$. This model-plate combination is also elevated from the channel floor by $\sim 0.68h$ to avoid the ground boundary layer from affecting the flow across model. Experiments are performed over a range of model yaw angles ($0^\circ - 15^\circ$) and Reynolds numbers Re_h, based on the freestream velocity and model height ($Re_h \sim \mathcal{O}[10^3 - 10^4]$). The yaw angle ($\beta$) is defined classically as the angle between the incoming flow direction and Ahmed body main axis. Hydrogen bubble-flow visualizations are performed in the horizontal plane at mid-body height to characterize the flow in terms of separation along lateral sides of the body and wake development. A 50 μm stainless steel wire mounted taut between 2 supports is used as cathode– source of hydrogen bubbles when supplied with a voltage of 80 V from a regulated power source. The wire is located just at the front of body and in contact with the leading face to seed the boundary layer developing on the model. Pulsed or continuous bubble sheets can be generated using a computer-controlled electronic switch. Image acquisition is through a 2048$\times$2048 pixels USB3 camera operating at 80 Hz.

For force measurements, the entire setup was mounted in an inverted direction, i.e. the model was suspended from a vertical strut and connected to a piezoelectric load-cell rated for 10 N and with a resolution of 0.002 N. The blockage ratio, computed as the ratio of model area to the water channel cross-sectional area was 5% when $\beta = 0^\circ$, and increases with yaw reaching around 9% at $\beta = 15^\circ$, the maximum yaw angle tested here. All the force measurements were conducted at $Re_h = 16 \times 10^3$, while the flow visualizations at Re_h of 8×10^3 in order to elaborate on the various flow structures observed

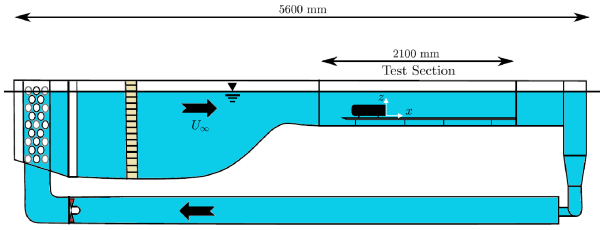

Figure 1. Experimental setup

on Ahmed body in yaw, operating both with and without flaps. Figure 1 presents the experimental setup. Rectangular flaps spanning 3 cm in length (s), height equal to that of the Ahmed body, and deflection of $\pm 5^\circ$ (measured w.r.t. the flow direction) were fabricated and fixed onto the vertical edges of the Ahmed body. These dimensions were selected based on the results in literature wherein flaps with these specific dimensions ($s/l = 10.3\%$) presented the best trend in drag reduction.

RESULTS & DISCUSSION

The model was mounted within the water channel such that the main axis of the body is aligned with the channel axis, thus ensuring that the model was equidistant to the channel sidewalls, and the model yaw angle implemented using a servo. The specified yaw angle and the actual implemented yaw angle were compared using a camera, the difference being less than $\pm$ 0.25°. The force data from the piezoelectric sensor was sampled at 1 kHz, and the measured force signal filtered to account for the effect of noise and drift. The filtered drag force signal was averaged (F) and non-dimensionalized using dynamic pressure and the exposed area (A, at $\beta = 0^\circ$) to obtain drag coefficient, as seen in equation 1 and ρ being fluid density. The data was acquired for 180 seconds at each yaw angle, the acquisition undertaken after the flow unsteadiness due to model rotation minimized.

$$C_D = \frac{F}{\frac{1}{2}\rho U_\infty^2 \cdot A} \tag{1}$$

Reynolds number ($Re_h = \rho U_\infty h/\mu$) is calculated based on model height and μ the dynamic viscosity of water.

Effect of yaw and vertical flaps on horizontal forces

Over the years significant amount of numerical and experimental studies on ground vehicles have been conducted. This has resulted in a wide range of datasets involving various configurations of Ahmed body– square-back, slant-back, base cavity profiles, and deflector configurations amongst others, over different Reynolds numbers. However, there are limited works on Ahmed body in cross-flow. Figure 2 presents the variation of drag coefficient with yaw angle of the different configurations under consideration here. The -5° flap angle corresponds to the scenario wherein flaps are directed towards the model centerline, while +5° flap angle the opposite. From figure 2, it can be observed that C_D for all the configurations increases with yaw, as expected. This is due to the creation of pressure difference about the lateral model faces (windward and leeward flow regions) with yaw, resulting in drag force increase. The plot also highlights the fact that the drag generated by the +5° flap configuration is consistently higher than that by

the square-back or -5° flap configurations. In terms of magnitude, the drag values obtained over these experiments are consistent with that available in literature. Lorite-Díez *et al.* (2020) have conducted wind-tunnel tests to study the effect of base cavity profiles on drag and compared it against a square-back model at $Re_h = 10^5$ over yaw angles 0° to 10°. Their measurements for square-back configuration match well with the current data. Verzicco *et al.* (2002) and Grandemange *et al.* (2015) have conducted numerical and experimental studies on square-back configuration without yaw at Re_h of 10^5 and 10^6 respectively, and the results are well in agreement. Although the experiments by Bello-Millán *et al.* (2016) are on Ahmed body with a slant-back profile at $Re_h = 2 \times 10^5$, the change in magnitude of model blockage and the associated drag rise with yaw are similar to that in current experiments. Owing to the absence of ground plate in the current force experiments, it is essential to eliminate the effect of free surface waves from drag values. Based on the works of Chaplin & Teigen (2003) on vertical, surface piercing cylinders and by Satheesh & Huera-Huarte (2019) on the effect of free surface on flat plates of different aspect ratios operating in cross-flow, it has been found that a model generates approximately 25% higher drag near the free surface than when located away from the boundaries. These results are applicable over a specific range of Reynolds numbers ($\mathcal{O}[10^3 - 10^5]$) and Froude numbers and has been utilized in the current measurements to minimize the contribution of wave drag to the total drag. Although the results by Tran *et al.* (2022) mention insensitivity in drag over a small range of yaw angles for a slant-back Ahmed body, no such trends have been observed in the current scheme. This is due to greater yaw angle resolution and lower blockage ratio in their work compared to the current one. However, their drag coefficients at low yaw angles are close to the current measurements.

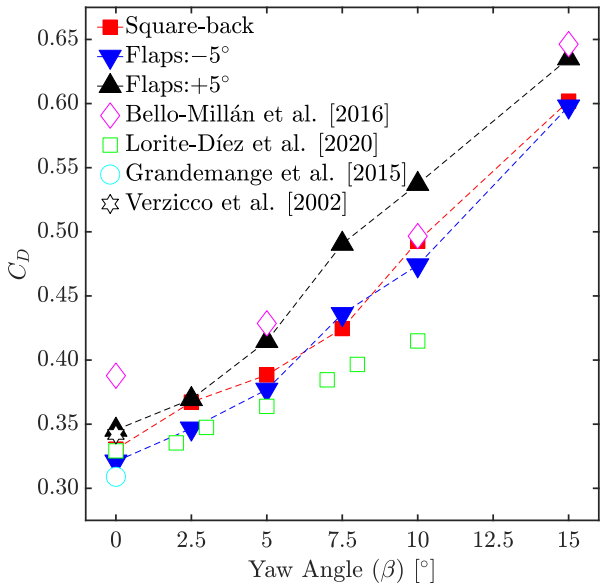

Figure 2. Drag coefficient variation with yaw for different Ahmed body configurations

Yaw effect

Even though Reynolds numbers provided by water tunnels are lower than those by wind tunnels, the ability to correlate the visualized flow structures with the measured forces are of greater benefit in this scenario wherein identifying the effect of vertical flap on the flow around body is the prime objective. Thus, the model roof was imaged in different configurations to study the flow. Image-averaging was undertaken to sort the instantaneous flow structures from long-term ones. Sectors of higher light intensity indicate regions wherein the observable flow structures are steady, while the diffuse regions are an indication of increased mixing and/or flow separation. The images for one of the configurations is inset in figures 3a and 3b to highlight the presence of conical vortices– one that extends along the model length, and another that undergoes skewing. It is observed that the conical vortices gain prominence with increasing yaw, with significant skewing of one of these vortices. Most of the previous visualizations have focused on the wake in order to correlate them with the measured force trends and not much attention given to flow across the model roof, especially the conical vortices and their skewing. Figure 3a presents a plot indicating the change in flow separation location with yaw on the leeward side, for different configurations. The separation location is measured with respect to the model front-face and non-dimensionalized using model length, the separation location being measured from images post averaging. Therefore $x/l = 0$ corresponds to a scenario where the flow separation occurs at the leading edge of the model while $x/l = 1$ to when the separation occurs at model's trailing edge. The plot indicates that the separation point moves upstream with yaw in all configurations, as expected. It also indicates that the presence of flaps has an influence on the separation point, forcing it further upstream when compared to the square-back configuration. No measurements have been performed on the windward side due to the absence of flow separation post a particular yaw angle. Similarly, figure 3b presents the location of skewed conical vortex, measured with respect to the left lateral edge of model and non-dimensionalized using model width. It is explicitly clear from this plot that vortex skewing increases with yaw in all configurations, its magnitude higher when flaps are used. From the inset images of $\beta > 0°$, it is also seen that the origin of skewed vortex is on the leading edge/face of body.

Effect of vertical flaps & yaw

Figure 4 presents instantaneous snapshots (viewed from underneath) highlighting the effect of yaw on Ahmed body models at a fixed Re_h. Each column corresponds to a particular yaw angle, and each row to a specific model configuration– square-back, and with flaps at fixed deflection angles ($\mp 5°$). Even from these instantaneous results, it is observed in all configurations that an increase in model yaw angle results in wake to be yawed as well, as expected. The interesting part is the presence of conical vortex (observed in background, on the roof) that appears prominently when the yaw angle is 10°, with this feature being more conspicuous in models with flaps (figures 4f and 4i). Flow separation and/or reattachment on leeward sides in all configurations is also apparent with the increase in yaw angle (figures 4c, 4f, 4i).

Figure 5 presents a set of time-averaged flow visualization images obtained in order to observe the variation in flow evolution and existing wake structures over a range of model yaw angles, Re_h being fixed at 8×10^3. It is observed that all the model configurations present a strong flow from the model roof into the wake. The flow is laterally symmetric, as expected when there is no yaw. Increasing the yaw angle results in an asymmetry– leading to observable conical vortices that extend along the entire model length, and the skewed vortex. This is observed in all the model configura-

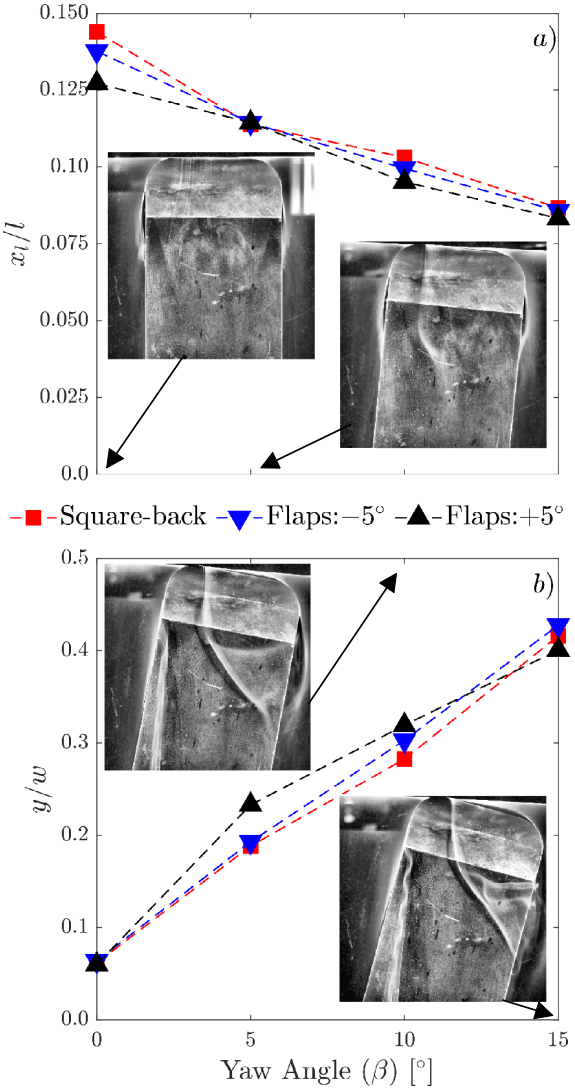

Figure 3. Variation with yaw of (*a*) flow separation location on leeward side and (*b*) conical vortex skew location

tions, their prominence increasing with yaw. Another aspect observed from the images is that the angle subtended by the conical vortex that extends along the body length always lags the model yaw angle. Studies (Large Eddy Simulation) by Krajnović & Davidson (2005) and experiments by Spohn & Gilliéron (2002) involving electrolytic precipitation/ tin-flow technique on a slant-back Ahmed body without yaw at Re_h of 2×10^5 and $\sim 8\times10^3$, respectively presents a detailed explanation regarding the different flow structures around Ahmed body and the effect of slant-edge on the flow. These works discuss the dynamics and trajectory of a conical vortex ($T_{r,l}$ vortex systems in Krajnović & Davidson (2005)) in the presence of a slant-edge, indicating that the existence of conical vortex and its extension along the entire model length. However, what is explicitly clear from the current work is that the conical vortex is not specific to a model geometry, and its evolution is dependent on model yaw.

Although the flow topology for the slant-back model has been well described by several researchers, results are non-existent for the square-back model, especially in cross-flow condition. Besides force measurements, the work by Tran *et al.* (2022) also estimated skin-friction drag on slant-back Ahmed body using a luminescent oil, and report the extension of conical vortex along the model length, and moves inward towards model centerline at the slant surface, with increasing model yaw. This results in increased interaction between the conical vortex and the separated flow on the slant surface, and is expected to be the source of increased drag. However, no such flow separation on roof of the square-back model (vis a vis slant-back model) is known to exist. The flow topology is further affected with the incorporation of vertical flaps, as can be observed from figures 4c, 4f and 4i. Apart from this, the skewing of conical vortex and its dependence on yaw is an unobserved measurement hitherto. The work of Lorite-Díez *et al.* (2020) involving detailed force and pressure measurements on a square-back model indicates a linear correlation between base pressure coefficient and the horizontal force coefficient, and their PIV measurements indicate development of an asymmetric recirculating flow that increases with yaw. However, further experiments are needed to ascertain whether all the drag rise associated with yaw can be attributed only to the yaw-induced wake asymmetry or if the skewed vortex also has a significant contribution. Thus, the current visualizations attest to the fact that flow topology on a square-back model in cross-flow is different compared to a slant-back.

CONCLUSIONS

The results obtained over these set of experiments involving a square-back Ahmed model and with vertical flaps in cross-flow have provided an unique insight into the forces and flow structures observed on model roof. The increase in drag with yaw for all the models is as expected, both in its trend and magnitude. The conical vortices highlight the flow transition occurring on the model roof with increasing yaw. One of the conical vortex extend downstream into the wake in all configurations, with its angle always lagging the imposed yaw angle. The instantaneous global flow and the time-averaged wake flow visualizations also indicate the prominence of conical vortex in cross-flow conditions. Meanwhile, another conical vortex skews increasingly with yaw, its skewing angle dependent on the presence of vertical deflectors. The skewing process is expected to be directly related to the imposed yaw angle. However, further experiments are necessary to elucidate this aspect and the reason for lag between the imposed yaw angle and the conical vortex extending along the model length, and are points of interest for future research. In all, the current force measurements and flow visualization conducted at $Re_h \sim \mathcal{O}[10^4]$ are in good agreement with literature wherein Re_h are even higher ($\mathcal{O}[10^5 - 10^6]$).

ACKNOWLEDGMENTS

The present work is funded by the French organization ANR under the project COWAVE ANR-17-CE22-0008.

REFERENCES

Ahmed, S. R., Ramm, G. & Faltin, G. 1984 Some salient features of the time-averaged ground vehicle wake. *SAE Transactions* pp. 473–503.

Beaudoin, J. F. & Aider, J. L. 2008 Drag and lift reduction of a 3D bluff body using flaps. *Experiments in fluids* **44** (4), 491–501.

Bello-Millán, F. J., Mäkelä, T., Parras, L., Del Pino, C. & Ferrera, C. 2016 Experimental study on Ahmed's body drag coefficient for different yaw angles. *Journal of Wind Engineering and Industrial Aerodynamics* **157**, 140–144.

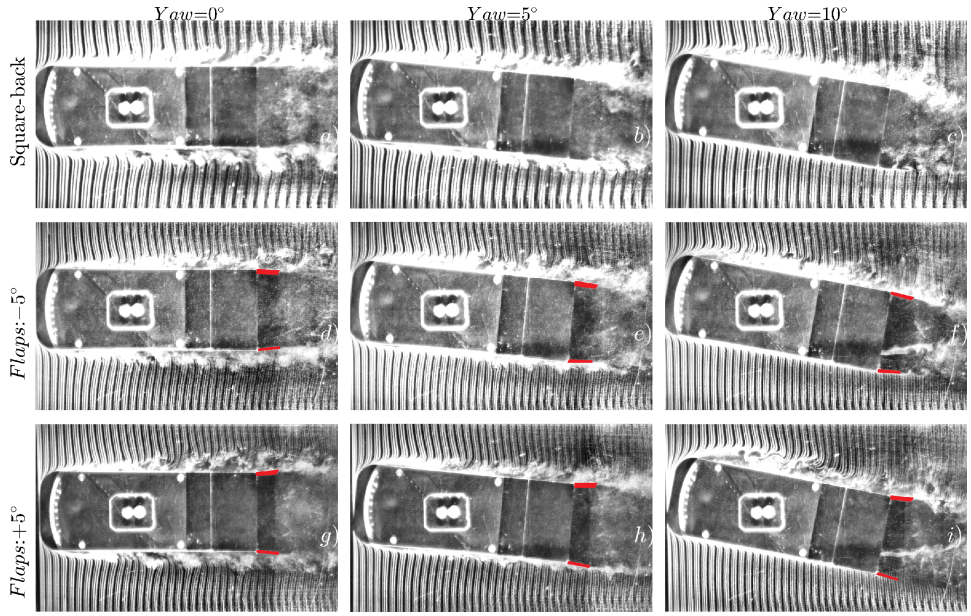

Figure 4. Instantaneous flow around different Ahmed body configurations at $Re_h = 8 \times 10^3$ (flaps highlighted in red) and different yaw angles

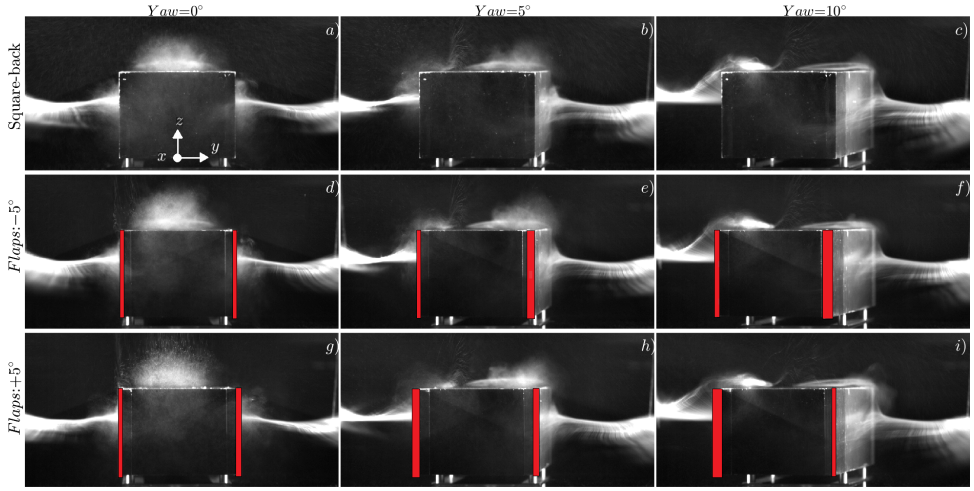

Figure 5. Time-averaged hydrogen bubble-flow visualization of Ahmed body wake plane in various configurations at $Re_h = 8 \times 10^3$

Chaplin, J. R. & Teigen, P. 2003 Steady flow past a vertical surface-piercing circular cylinder. *Journal of Fluids and Structures* **18** (3-4), 271–285.

de la Cruz, J. M. G., Brackston, R. D. & Morrison, J. F. 2017 Adaptive base-flaps under variable cross-wind. *Tech. Rep.*.

Fourrié, G., Keirsbulck, L., Labraga, L. & Gilliéron, P. 2011 Bluff-body drag reduction using a deflector. *Experiments in Fluids* **50** (2), 385–395.

Grandemange, M., Cadot, O., Courbois, A., Herbert, V., Ricot, D., Ruiz, T. & Vigneron, R. 2015 A study of wake effects on the drag of Ahmed's squareback model at the industrial scale. *Journal of Wind Engineering and Industrial Aerodynamics* **145**, 282–291.

Krajnović, S. & Davidson, L. 2005 Flow around a simplified car, part 2: understanding the flow. *Journal of Fluids Engineering* .

Littlewood, R. & Passmore, M. 2010 The Optimization of Roof Trailing Edge Geometry of a Simple Square-Back. *Tech. Rep.*.

Lorite-Díez, M., Jiménez-González, J. I., Pastur, L., Cadot, O. & Martínez-Bazán, C. 2020 Drag reduction on a three-dimensional blunt body with different rear cavities under cross-wind conditions. *Journal of Wind Engineering and Industrial Aerodynamics* **200**, 104145.

Satheesh, S. & Huera-Huarte, F. J. 2019 Effect of free surface on a flat plate translating normal to the flow. *Ocean Engineering* **171**, 458–468.

Spohn, A. & Gilliéron, P. 2002 Flow separations generated by a simplified geometry of an automotive vehicle. In *IUTAM Symposium: unsteady separated flows*, , vol. 1. Kluwer Academic.

Tran, T. H., Anyoji, M., Nakashima, T., Shimizu, K. & Le, A. D. 2022 Experimental Study of the Skin-Friction Topology Around the Ahmed Body in Cross-Wind Conditions. *Journal of Fluids Engineering* **144** (3).

Verzicco, R., Fatica, M., Iaccarino, G., Moin, P. & Khalighi, B. 2002 Large eddy simulation of a road vehicle with drag-reduction devices. *AIAA journal* **40** (12), 2447–2455.